https://doi.org/10.1016/j.tws.2018.11.024

Structural performance of cold-formed steel elliptical hollow section pin-ended columns

Man-Tai Chen [a*], Ben Young [b]

[a, b] *Department of Civil Engineering, The University of Hong Kong, Pokfulam Road, Hong Kong, China.*

Abstract

The structural performance of cold-formed steel elliptical hollow section pin-ended columns buckled about the minor axis was studied through experimental and numerical investigation. Four cross-section series with five different column lengths were designed in the test program to include a wide range of cross-section geometries and column slenderness. Finite element model was developed to replicate the key test results and to perform extensive parametric study. The validation results show that the model can accurately predict the behavior of cold-formed steel elliptical hollow section pin-ended columns buckled about the minor axis. Subsequently, an extensive parametric study with a wide range of cross-section geometries and a spectrum of column slenderness was performed. Since currently there is no codified design rule on elliptical hollow section compression members, the results of 22 column tests and 280 finite element analyses were only compared with the predicted strengths by the equivalent diameter method and equivalent rectangular hollow section approach proposed by previous researchers, the traditional design methods with equivalent diameter incorporated as well as the Direct Strength Method. Reliability analysis was conducted to examine these design methods. Among these design methods, the comparisons show that the existing Direct Strength Method offers the most suitable design provisions, though further improvement remains possible. In this study, modification was proposed on Direct Strength Method to further improve the accuracy of the design strength predictions. It is suggested to adopt the modified Direct Strength Method design equations in the nominal strength predictions of cold-formed steel elliptical hollow section pin-ended columns buckled about the minor axis.

Keywords: Cold-formed; Direct strength method; Elliptical hollow section; Pin-ended columns; Structural design.

---

[*] Corresponding author. Tel.: +852-6925-0119; fax: +852-2559-5337.

E-mail address: cmt111@connect.hku.hk (M.T. Chen).

1. Introduction

Elliptical hollow section (EHS), as a recently emerged cross-section type, has the complementary qualities of aesthetic appearance and the sound structural efficiency evident by the streamline profile and the possession of different major and minor geometric properties, respectively. The EHS members have been employed recently as structural supporting components in various types of structures, such as the glass roof supporting members in International Finance Center in Hong Kong (Fig. 1a), the glass facade supporting members in Heathrow Airport in London (Fig. 1b), the main building in Terminal 4 of Barajas Airport in Madrid, the society bridge in Braemar, Honda central sculpture in Goodwood and the office building in airside business park in Ireland. However, the lack of design procedure for this relatively new section has yielded overly conservative design by engineers. This has prompted research aiming at studying the behavior of EHS structural members [1-14].

Chan and Gardner [1-3] have conducted experimental and numerical investigation on the structural behavior of hot-finished steel elliptical hollow sections under bending and uniform compression. The shear response of hot-finished steel EHS [6], lateral instability of hot-finished steel EHS beams [9], buckling behavior of EHS beam-column members [10] as well as plastic collapse mechanism of EHS under compression [8] have been investigated. Based on the research findings of hot-finished steel EHS, design methods have been proposed for hot-finished EHS members under various loading conditions [4, 5, 7]. In addition, Theofanous *et al*. [11, 12] investigated the structural response of stainless steel EHS beams and columns through both experimental and numerical studies. Nonetheless, the majority of research studies on EHS have been focused on the behavior of hot-finished steel and cold-formed stainless steel EHS. Recently, Chen and Young [13, 14] have studied the material properties and cross-sectional behavior of cold-formed steel EHS. However, the research studies on cold-formed steel EHS structural members are very limited [13, 14].

This paper aims at investigating the structural performance of cold-formed steel elliptical hollow section pin-ended columns buckled about the minor axis. In the experimental investigation, twenty-two column tests were conducted between pinned ends with the designed specimen lengths varying from 200 mm to 1500 mm to cover a spectrum of column slenderness. The results obtained from test program were employed in the validation of finite element (FE) model. Subsequently, an extensive parametric study comprising 280 finite element analyses on cold-formed steel EHS pin-ended columns buckled about the minor axis was performed based on the verified model. Since the current design specifications for steel structures [15-19] do not cover the design of cold-formed steel EHS compression members, the experimental and numerical results obtained in this study were only compared with the predicted strengths by the equivalent diameter method [4], the equivalent rectangular hollow section (RHS) approach [7], the traditional design rules originally developed for circular hollow section [15-17] with equivalent diameter incorporated as well as the Direct Strength Method (DSM) [15]. Modification on DSM is proposed in this study. The applicability and reliability of the existing and modified design methods were evaluated through reliability analysis.

2. Experimental investigation

2.1. Pin-ended column specimens

The test specimens consisted of 22 pin-ended columns. The test specimens are categorized into four series according to the cross-section geometries of EHS. The formation process for each series has been described by Chen and Young [13]. The nominal dimensions ($D\times B\times t$) of EHS are 140×85×3, 150×50×5, 150×70×3 and 180×65×5, where D, B and t are the larger outer diameter, the smaller outer diameter and the wall thickness of the section, respectively. The nominal cross-section aspect ratio of EHS (D/B) covers a wide range from 1.65 to 3. The material properties were determined by conducting tensile coupon tests on specimens extracted from the flattest and the curviest portions of each EHS. The details and results of tensile coupon tests were discussed and reported by Chen and Young [13], whilst a summary of the obtained material properties is presented in Table 1. All the EHS specimens are labeled such that the nominal cross-section

geometries, the specimen type and the specimen length can be identified. The letters C in the last part of the specimen label indicates a pin-ended column. The following letter L together with the number designates the length of the actual specimen, whereas the symbol # denotes a repeated test. The measured specimen dimensions are reported in Table 2.

2.2. Geometric imperfection measurements

Prior to the column tests, initial global geometric imperfections ω_g of the cold-formed steel EHS pin-ended columns were obtained based on the measurements taken on the locations with the smallest curvature (at the tips of major axis) at mid-height and near both ends of the specimens in the buckling direction (minor axis buckling) using a Leica TCR405 total-station prior to testing. The initial global imperfection is positive when the specimen is bowed in the same direction as the bending direction, and vice versa. The measured initial global imperfection was normalized by the actual specimen length. The measured and normalized values of initial global imperfection are reported in Table 2. The average absolute value of the normalized initial global imperfection at mid-length (ω_g/L) was 1/4605 for the test column specimens. The negligibly small value of initial global geometric imperfection demonstrates the great straightness of the tubes.

2.3. Test setup and procedure

Twenty-two cold-formed steel EHS columns were compressed between two pinned ends to examine the load-carrying capacity, load-end shortening history and failure mode of the column specimens. The column samples were cut to specified specimen lengths of 200, 440, 850, 1200 and 1500 mm with both ends milled flat before welding of 25.4 mm thick end plates.

The test setup and test rig of pin-ended columns of various lengths are shown in Figs. 2 and 3. A pair of pin-ended special bearings was designed and used to replicate the pinned end conditions and to allow free rotations about the minor axis as well as to restrain rotations about the orthogonal axis. Each of the pin-ended special bearing comprises one pit plate with V-shaped groove and one wedge plate with knife-edge. For the test setup of columns with actual specimen lengths of 850,

1200 and 1500 mm, the upper pit plate was fixed and the lower one was installed on a special ball bearing at the bottom as shown in Fig. 3. The slotted wedge plates allow the adjustment of the specimen to achieve concentric loading condition. Before testing, the upper and lower pit plates were positioned in-line. A small preloading of 3 to 5 kN was then applied to eliminate any possible gaps between the wedge plates and the pit plates as well as to ensure everything was in full contact and the specimen was in an up-right position. Twisting and rotation of the special ball bearing were restrained by locking the horizontal and vertical bolts, respectively. Another hydraulic testing machine was used for the short column tests with actual specimen lengths of 200 and 440 mm. The test setup is similar to that for other column tests but a different lockable sitting was adopted as shown in Fig. 2.

Three LVDTs were installed to measure both the end shortening and end rotation of the specimens. In addition, two LVDTs were installed horizontally at the mid-height of the specimen on the two sides in the bending plane to capture the real-time horizontal deflection of the columns during loading. To determine the loading eccentricity, two strain gauges were attached on two faces in the bending plane at the mid-height of each specimen, at which the extreme compressive and tensile fibers located. Displacement controlled loading method was used to drive the hydraulic actuator at a constant speed of 0.3 mm/min to apply the axial compression to the specimens. The static responses of specimens can be obtained by pausing the applied displacement for 100 seconds near the ultimate load. The load, readings from LVDTs and strain gauges were recorded at one second intervals by a data acquisition system.

The readings of strain gauges together with the applied load and lateral deflection in the bending direction at mid-height of the column were recorded to determine the actual loading eccentricity of the specimen. Within the elastic range, the bending moment of the specimen at mid-height caused by the unintentional eccentricity can be expressed as $P(e+\omega_g+\Delta)$ or $EI_y\kappa$. By equating these two expressions, the measured loading eccentricity with the initial global geometric imperfection can be determined by $(e+\omega_g)=EI_y\kappa/P-\Delta$, where EI_y is the flexural rigidity of the

cross-section about the bending axis, κ is the curvature of the specimen and is expressed as the strain gradient of the section under bending, P is the applied compressive load, e is the eccentricity at specimen ends, ω_g is the initial global geometric imperfection and Δ is the lateral deflection of specimen at mid-height in the bending direction. When the column specimen was preloaded within the elastic range, the position of specimen was adjusted until the readings of two strain gauges located at extreme fibers were close to each other. Though the targeted eccentricity of column specimen was zero, there still existed an unintentional eccentricity for each specimen, the values of which are reported in Table 3. The excellent alignment of the column specimens was demonstrated by the average measured eccentricity of 0.25 mm in this study.

2.4. Test results

The key test results of cold-formed steel EHS column specimens, including the load-carrying capacities and failure modes are reported in Table 3. The effective length (L_e) of the pin-ended column was measured between the tips of knife-edged wedges at two ends as shown in Figs. 2 and 3, and was calculated as the sum of specimen length, the thicknesses of two end plates (50.8 mm) and the heights of the two wedge plates (122.8 mm). Different failure modes were observed in the pin-ended column tests, such as material yielding (Y), local buckling (L), flexural buckling (F) as well as interaction of local and flexural buckling (L+F) as reported in Table 3. To identify material yielding failure of column, the ultimate column strength was compared with the squash load (P_y) of the column specimen, which was calculated as the product of the 0.2% proof stress of material at the flattest portion and the total cross-section area. The column was considered to fail by material yielding when the ultimate strength was greater than the squash load of the column specimen in this study. It can be observed from Table 3 that the ratio of ultimate strength to squash load for most of EHS short column specimens with actual specimen lengths of 200 and 440 mm was greater than unity, excluding the EHS with nominal cross-section dimensions of 140×85×3, for which the ratio of P_{Exp}/P_y was approximately equal to, but less than unity. These indicate that most of EHS short columns failed by material yielding, except that the EHS short columns with the nominal cross-section dimensions of 140×85×3 failed by local buckling. The flexural buckling failure

started to appear as column length increases. The static load-end shortening responses for typical EHS pin-ended column specimens are depicted in Fig. 4.

3. Numerical investigation

3.1. Basic modeling parameters and assumptions

In conjunction with the experimental investigation, numerical modeling was performed by using the finite element analysis program ABAQUS of version 6.14 for model validation and parametric study. The measured cross-section geometries and material properties as reported in Tables 1 and 2 were incorporated in the finite element model, and full length of actual column specimen was modeled.

The four nodes shell element with reduced integration (S4R) was selected as the element type throughout the numerical investigation. The minimum of 20 mm and $B/20+(D-B)/10\pi$ was taken as the mesh size of the model. The mesh was assigned uniformly in circumferential and longitudinal directions of the EHS column model.

The pin-ended boundary condition and the effective length of the test column specimen were simulated by coupling the displacements of cross-section edges at both ends of column specimen to the displacements of the corresponding reference points located 86.8 mm, which is the sum of the end-plate thickness and the height of one wedge plate, away from the specimen edges. The reference points were offset from the centroid of the cross-section in the finite element model to cater for the unintentional loading eccentricity. All degrees of freedom of the reference points were restrained, excluding the longitudinal displacement at the loading point and the minor axis rotation at two ends. The compressive load was applied by specifying the axial displacement of the reference point at the loading end using a static RIKS step. The nonlinear geometric parameter (*NLGEOM) was enabled to allow for large displacement analysis.

The residual stresses were introduced to the section during the cold-rolling and welding

processes. For the inclusion of residual stress, since the bending residual stress, which has the larger magnitude and more significant effect compared to the membrane residual stress [13, 20], has already been included into the measured material properties obtained from coupon tests, explicit inclusion of residual stresses in the FE model was deemed to be unnecessary [13, 20-25].

In general, the curviest portion of the EHS underwent more cold-work than the flattest portion, which results in a more significant material strength enhancement in the curviest portion. Similar sensitivity analysis as conducted by Chen and Young [13] on the distribution of material properties obtained from the flattest and curviest portions of EHS was conducted in this study. The strength enhancement of EHS at the curviest portion was extended from the tip of the section to a certain distance. Different fractions of the larger dimension of the median-profile of the sections (D_m/3, D_m/4, D_m/6 and D_m/10) were included in the sensitivity analysis. The results of the sensitivity analysis show that FE strengths based on different material properties distributions are similar with the difference of only 2% as reported in Table 4. Therefore, the same fraction value of D_m/6 as used in the cold-formed steel EHS stub column model [13] was adopted. This value of strength enhancement was used in the model validation and further parametric study.

For the consideration of geometric imperfections, proper buckling mode shapes should be carefully selected as it would influence the buckling behavior of EHS structural members [26, 27]. In the modeling, the lowest elastic local and global buckling mode shapes determined by eigenvalue analysis were taken as the corresponding imperfection patterns along the specimen length. The local and global buckling mode shapes were amplified by the corresponding magnitudes and were further superimposed on the column finite element model. Sensitivity study was conducted by considering four magnitudes of local imperfection (t/3, t/10, t/50, and t/100) with a fixed value of global imperfection (L/3500) as shown in Table 4 to determine the suitable magnitudes of the imperfections. To be consistent with the finite element model for cold-formed steel EHS stub columns [13], the magnitude of t/50 was selected for local imperfection in the model. For global imperfection of column specimen, the magnitude of L/3500 was selected.

3.2. Validation of finite element model

On the basis of the aforementioned modeling parameters and assumptions, the finite element model of cold-formed steel EHS pin-ended column buckled about the minor axis was developed and validated against 22 column tests. Key results obtained from the test program, including ultimate load-carrying capacity, full load-end shortening response and failure mode, were compared with those obtained from the numerical analyses. The accuracy of the FE model was evaluated by means of test-to-FE strength ratio. The validation results for the finalized numerical model are shown in the second last column of Table 4. The mean value and coefficient of variation (COV) of the test-to-FE strength ratio are 1.03 and 0.073, respectively. This demonstrates that the finite element model can successfully replicate the load-carrying capacities of the cold-formed steel EHS pin-ended columns buckled about the minor axis. The comparisons of load-end shortening responses obtained from the test and finite element analysis for column specimens failed by different failure modes, including local buckling, interaction of local and flexural buckling, material yielding, and flexural buckling are presented in Figs. 5-8, respectively. The failure modes can also be captured in the FE analysis as shown in Figs. 9-11.

3.3. Parametric study

Material properties at the flattest and curviest portions of EHS 140×85×3 were used in the parametric study. An extensive parametric study comprising 280 finite element analyses on cold-formed steel EHS pin-ended columns buckled about the minor axis was performed based on the verified model. Fifty-six different cross-sections with five different column lengths for each section were included in the finite element analyses. A broad range of cross-section geometries and column slenderness was designed for the parametric study. The cross-section aspect ratio of the EHS varied from 1.25 to 3.50 and the larger dimension of the section (D) varied from 150 to 500 mm. The equivalent diameter (D_e) and cross-section slenderness (D_e/t) defined by Chan *et al.* [4] for EHS columns buckled about the minor axis were adopted to examine the coverage of cross-section slenderness in the parametric study. The cross-section slenderness covers a wide

range from 16 to 490 and the lengths of the column specimens were designed to cover a spectrum of column slenderness ($\lambda=L_e/r$) ranging from 12.5 to 131.3. The ultimate load-carrying capacities of column specimens obtained from the numerical study are summarized in Table 5.

4. Reliability analysis

The reliability of the equivalent diameter method [4], the equivalent RHS approach [7], the current traditional design rules [15-17] with equivalent diameter incorporated as well as the existing and modified Direct Strength Method for the design strength predictions of cold-formed steel EHS pin-ended columns buckled about the minor axis was evaluated through reliability analysis. Reliability analysis is detailed in the North American Specification AISI-S100 [15]. A target reliability index (β) of 2.5 for structural steel members was adopted, below which the design rules are considered to be unreliable. The values of resistance factors (ϕ) adopted in different design methods are shown in Table 6. The load combination of 1.35DL+1.5LL was used for the equivalent diameter method and equivalent RHS approach, while 1.2DL+1.6LL was used for the North American (including the DSM) and American Specifications. For Australian Standard, the load combination of 1.2DL+1.5LL was adopted in the reliability analysis, where DL and LL mean the dead load and live load, respectively. The resistance factor together with the calibration coefficient determined by the load combination specified in different design specifications [15-17, 19] and the statistical parameters as specified in the AISI-S100 [15] were used in the calculation of reliability index. The reliability indices of existing and modified design rules for nominal strength (unfactored design strength) predictions of cold-formed steel EHS pin-ended columns are shown in Table 6.

5. Current design methods and comparison of column strengths

5.1. General

The material properties at the location with lowest 0.2% proof stress were used in nominal strength calculation for conservative predictions. The traditional design rules for structural steel design [15-19] do not cover the design of cold-formed steel EHS compression members. Therefore,

the load-carrying capacities of cold-formed steel EHS pin-ended columns obtained from experimental and numerical studies were compared with the design strengths (unfactored design strengths) predicted by the equivalent diameter method [4] and the equivalent RHS approach [7] previously proposed for the design of hot-finished steel elliptical hollow sections as well as the traditional design methods developed for CHS [15-17] with equivalent diameter incorporated and the DSM [15].

Before evaluating the nominal axial strengths of pin-ended columns, the effect of the additional bending moments induced by the unintentional eccentricities on the design strengths was quantified by comparing the column design strengths calculated by considering the ideal case with zero eccentricity with the counterpart calculated by considering the measured eccentricities ($e+\omega_g$). Since no existing design rule is available for the cold-formed steel EHS investigated in this study, the interaction equation for member under combined compression and bending as specified in the ANSI/AISC360 [16] was adopted for design strength calculation. The nominal axial and flexural strengths involved in the interaction equation were determined from the design equations developed for circular hollow section (CHS) in the ANSI/AISC360 [16] by adopting the equivalent diameter proposed by Chan *et al.* [4]. Based on this methodology, the difference between the two calculations, one for column with zero eccentricity and another for counterpart with measured unintentional eccentricity, is only 1.8% on average for the axial strength. The small difference indicates that the columns were properly aligned and the effect of unintentional eccentricity on column strength prediction is negligibly small.

The results of previous research studies revealed that the structural behavior of EHS columns is influenced by the cross-section aspect ratio of EHS [8, 26, 28, 29]. In this study, the test and FE strengths of EHS columns were grouped by cross-section aspect ratio to examine the influence of aspect ratio on the structural behavior and the accuracy of design strength predictions of cold-formed steel EHS compression members.

5.2. Equivalent diameter method proposed by Chan *et al*. [4]

The equivalent diameter method proposed by Chan *et al.* [4] for the EHS compressive members together with the column buckling curve 'c' specified in the EN1993-1-1 [19] for cold-formed steel were used to predict the design strengths of cold-formed steel EHS pin-ended columns. The applicability of this method for design strength predictions of cold-formed steel EHS pin-ended columns was evaluated by comparing the experimental and numerical results with the design strengths predicted by the equivalent diameter method.

The comparison results are shown in Table 6 and Fig. 12. The equivalent diameter method provides very conservative and scattered design strength predictions for cold-formed steel EHS pin-ended columns with the mean value and corresponding COV of P_u/P_{Chan} being 1.59 and 0.251, respectively. The reliability index is 2.71 for the resistance factor of 1.0. These indicate that the design strength predictions by the equivalent diameter method proposed by Chan *et al.* [4] are reliable even though the predictions are very conservative and scattered.

5.3. Equivalent RHS approach proposed by Haque *et al*. [7]

The equivalent RHS approach for the design of EHS compressive members buckled about the minor axis was proposed by Haque *et al.* [7] based on the results of hot-finished steel EHS. By incorporating the column buckling curve 'c' for cold-formed steel as specified in the EN1993-1-1 [19], the feasibility of the equivalent RHS approach for the design of cold-formed steel EHS compressive members buckled about the minor axis was examined.

The load-carrying capacities of specimens obtained from tests and parametric study were compared with the design axial strengths predicted by the equivalent RHS approach proposed by Haque *et al.* [7] as shown in Table 6 and Fig. 13. The mean value of P_u/P_{Haque} is 1.56 with the corresponding COV of 0.387. The design strength predictions by the equivalent RHS approach are also very conservative and even more scattered compared to the predictions by the equivalent diameter method. The reliability index is 2.02 for the resistance factor of 1.0, indicating that the

equivalent RHS approach proposed by Haque *et al.* [7] is not reliable in predicting the design strengths of cold-formed steel EHS pin-ended columns buckled about the minor axis.

5.4. Existing traditional design rules with equivalent diameter incorporated

By incorporating the equivalent diameter proposed by Chan *et al.* [4] for EHS compressive members buckled about the minor axis, the existing traditional design rules originally developed for CHS in the Australian Standard [17], the North American [15] and American Specifications [16] were used to predict the design strengths of cold-formed steel EHS pin-ended columns buckled about the minor axis. For the predictions by the Australian Standard [17], compression member section constant (α_b) of -0.5 for cold-formed (non-stress relieved) RHS and CHS was adopted in the member slenderness reduction factor calculation. The upper limit of slenderness ratio (D_e/t) specified in different design rules to avoid uneconomic design was released to assess the applicability of the existing traditional design rules with equivalent diameter incorporated for the design strength predictions of cold-formed steel EHS pin-ended columns investigated in this study.

The axial strengths of column specimens obtained from experimental and numerical investigation were compared with the design strengths predicted by the Australian Standard [17], the North American [15] and American Specifications [16] with the equivalent diameter adopted. The comparison results are summarized in Table 6 and are depicted from Fig. 14 to Fig. 16. The mean values of $P_u/P_{AS4100}^{\dagger}$, $P_u/P_{AISI}^{\dagger}$ and $P_u/P_{AISC}^{\dagger}$ are 4.97, 1.17 and 1.18 with the corresponding COV of 2.106, 0.081 and 0.089 for design strengths predicted by the Australian Standard [17], the North American [15] and American Specifications [16], respectively. The reliability indices are 1.02, 3.30 and 3.09 for the resistance factors of 0.90, 0.85 and 0.90, respectively.

From the results, it is clear that by using the equivalent diameter proposed by Chan *et al.* [4], the Australian Standard [17] is not capable in predicting the design strengths of cold-formed steel EHS pin-ended columns buckled about the minor axis. The North American [15] and American Specifications [16] are able to provide more accurate and less scattered design predictions than the

equivalent diameter method [4] and the equivalent RHS approach [7]. However, the predictions are still quite conservative.

5.5. Direct strength method

The Direct Strength Method as detailed in the AISI-S100 [15] is a recently developed alternative design approach for steel structures and is recommended for its calculation efficiency since the cross-section classification and effective section calculation are no longer needed in the design strength predictions. The nominal axial strength is determined by the minimum of the nominal axial strengths for flexural, torsional or flexural-torsional buckling as well as local buckling and distortional buckling. No distortional buckling was observed for EHS. The finite strip method incorporated in CUFSM program [30], which is applicable to arbitrary cross-sections, was used to obtain the critical elastic column buckling load for local buckling. The critical elastic column buckling load for overall buckling was obtained in accordance with the AISI-S100 [15]. The obtained critical elastic column buckling loads for different buckling scenarios, namely local buckling and flexural buckling, were substituted into the DSM design equations to calculate the nominal axial strengths for different buckling scenarios, and the nominal axial strengths of the column specimens can be therefore obtained.

Since the DSM was originally calibrated for cold-formed steel open sections with plate elements, the applicability of the existing DSM for the design of cold-formed steel EHS pin-ended columns buckled about the minor axis is questionable and was therefore evaluated herein by comparing the results obtained from tests and finite element analyses with the design strength predictions. The comparison results are shown in Table 6, Figs. 17 and 18. The results show that the DSM provides the most accurate and least scattered design strength predictions for cold-formed steel EHS pin-ended columns among the existing design approaches as evident by the mean value and the corresponding COV of P_u/P_{DSM} being 1.05 and 0.048, respectively. The reliability index is 3.00 for the resistance factor of 0.85. The results indicate that the existing DSM as detailed in the AISI-S100 [15] provides accurate and reliable design strength predictions for cold-formed steel

EHS pin-ended columns buckled about the minor axis. However, further improvement remains possible.

6. Modified Direct Strength Method

The possibility of further improvement on the predictions by adopting the modified DSM design equations for local and overall buckling was reviewed. The relationship between P_{nl}*/P_y and the slenderness factor for local buckling (λ_l) proposed by Chen and Young [13] for cold-formed steel EHS stub columns as shown in Eq. (1) was adopted in the modified DSM. In addition, the DSM design curve for nominal overall buckling strength was modified as expressed by Eq. (2). The nominal strengths predicted by the modified DSM (P_{DSM}*) were equal to the minimum of P_{nl}* and P_{ne}* with consideration of local buckling and overall buckling, respectively. The slenderness factors for local (λ_l) and flexural buckling (λ_c) of column are defined in Eqs. (3) and (4), respectively.

$$P_{nl}{}^{*} = \begin{cases} 1.2P_y & \text{for } \lambda_l \le 0.178 \\ \left[1 - 0.16\left(\frac{P_{crl}}{P_y}\right)^{0.14}\right]\left(\frac{P_{crl}}{P_y}\right)^{0.14} P_y & \text{for } \lambda_l > 0.178 \end{cases} \quad (1)$$

$$P_{ne}{}^{*} = \begin{cases} \left(0.715^{\lambda_c{}^2}\right) P_y & \text{for } \lambda_c \le 1.17 \\ \left(\frac{0.825}{\lambda_c{}^{1.7}}\right) P_y & \text{for } \lambda_c > 1.17 \end{cases} \quad (2)$$

$$\lambda_l = \sqrt{\frac{P_y}{P_{crl}}} \quad (3)$$

$$\lambda_c = \sqrt{\frac{f_y}{f_{cre}}} \quad (4)$$

$$f_{cre} = \frac{\pi^2 E}{(L_e/r)^2} \quad (5)$$

where P_y is the squash load, P_{crl} is the critical elastic local buckling load of column, f_y is the yield stress and f_{cre} is the critical elastic flexural buckling stress as determined by Eq. (5).

The experimental and numerical results obtained from this study were compared with the

design predictions by the modified DSM as shown in Table 6, Figs. 18 and 19. The accuracy of nominal axial strength predictions is improved by adopting the modified DSM as evident by the mean value and the corresponding COV of P_u/P_{DSM}* being 1.01 and 0.023, respectively. The reliability index is 2.88 for the proposed resistance factor of 0.85, indicating that the modified DSM is reliable in predicting the nominal axial strengths for cold-formed steel EHS pin-ended columns buckled in minor axis.

7. Conclusions

The majority of recent research studies on elliptical hollow sections have been focused on the behavior of hot-finished steel and cold-formed stainless steel elliptical hollow sections, whilst the research studies on cold-formed steel elliptical hollow section structural members are very limited. In this study, both experimental and numerical investigation were carried out to study the structural performance of cold-formed steel elliptical hollow section pin-ended columns buckled about the minor axis. For the experimental investigation, a total of 22 column tests was conducted for different specimen lengths. The details of the test program, including the test set-up, procedure and key results, are described in this paper. For the numerical investigation, finite element model was developed and verified with the test results. An extensive parametric study comprising 280 finite element analyses was performed covering a broad range of cross-section geometries and column slenderness. With the results obtained from test program and numerical investigation, the feasibility of existing design methods, such as the equivalent diameter method, the equivalent rectangular hollow section approach as well as the existing design rules with equivalent diameter incorporated and the Direct Strength Method, was evaluated. Among these existing design methods, the assessment of results show that the Direct Strength Method offers the most accurate and the least scattered design strength predictions in a reliable manner. The possibility of further improvement on the design predictions was reviewed by adopting the modified Direct Strength Method design equations for local and overall buckling. With the modified design equation for flexural buckling proposed in this study, the accuracy of design strength predictions is improved. In this study, it is

recommended to adopt the modified Direct Strength Method design equations for the design of cold-formed steel elliptical hollow section pin-ended columns buckled about the minor axis.

Acknowledgements

The authors are grateful to Shenyang Dongyang Special Section Tube for supplying the test specimens. The research work described in this paper was supported by a grant from the Research Grants Council of the Hong Kong Special Administrative Region, China (Project No. 17267416).

Nomenclature

B	The smaller outer diameter of the section
COV	Coefficient of variation
D	The larger outer diameter of the section
D_e	Equivalent diameter of elliptical hollow section
D_m	The larger dimension of the median-profile of the section
DSM	Direct strength method
E	Young's modulus
e	Loading eccentricity
EHS	Elliptical hollow section
f_{cre}	Critical elastic buckling stress for flexural buckling
f_y	Yield stress
I_y	Moment of inertia about the bending axis
L	Total specimen length
L_e	Effective length of column
n	Ramberg-Osgood parameter
P	Applied axial compression

$P_{AISC}^{\dagger}$ Nominal axial strength predicted by American Specification ANSI/AISC360 [16] with equivalent diameter incorporated

$P_{AISI}^{\dagger}$ Nominal axial strength predicted by North American Specification AISI-S100 [15] with equivalent diameter incorporated

$P_{AS4100}^{\dagger}$ Nominal axial strength predicted by Australian Standard AS4100 [17] with equivalent diameter incorporated

P_{Chan} Nominal axial strength predicted by the equivalent diameter method proposed by Chan *et al.* [4]

P_{crl} Critical elastic local buckling load of column

P_{DSM} Nominal axial strength predicted by the Direct Strength Method

P_{DSM}* Nominal axial strength predicted by the modified Direct Strength Method

P_{Exp} Experimental loading capacity

P_{FE} Finite element loading capacity

P_{Haque} Nominal axial strength predicted by the equivalent RHS approach proposed by Haque *et al.* [7]

P_{ne}* Nominal axial strength of column for flexural buckling

P_{nl}* Nominal axial strength of column for local buckling

P_u Ultimate axial loading capacity

P_y Squash load of cross-section

r Radius of gyration

t Thickness of the section

TC Tensile coupon specimen

α_b Compression member section constant defined in the Australian Standard [17]

β Reliability index

Δ Lateral deflection of specimen at mid-height in the bending direction

ε_f Tensile strain at fracture

ε_u Tensile strain at ultimate

ϕ Resistance factor

κ	Curvature of the specimen
λ	Column slenderness
λ_c	Slenderness factor for flexural buckling
λ_l	Slenderness factor for local buckling
σ_u	Static ultimate tensile strength of material
$\sigma_{0.2}$	Static 0.2% tensile proof stress of material
ω_g	Initial global geometric imperfection

References

[1] Chan TM, Gardner L. Bending strength of hot-rolled elliptical hollow sections. Journal of Constructional Steel Research 2008;64(9):971-986.

[2] Chan TM, Gardner L. Compressive resistance of hot-rolled elliptical hollow sections. Engineering Structures 2008;30(2):522-532.

[3] Chan TM, Gardner L. Flexural buckling of elliptical hollow section columns. Journal of structural engineering 2009;135(5):546-557.

[4] Chan TM, Gardner L, Law KH. Structural design of elliptical hollow sections: a review. Proceedings of the Institution of Civil Engineers-Structures and Buildings 2010;163(6):391-402.

[5] Gardner L, Chan TM. Cross-section classification of elliptical hollow sections. Steel and Composite Structures 2007;7(3):185-200.

[6] Gardner L, Chan TM, Wadee MA. Shear response of elliptical hollow sections. Structures and Buildings 2008;161(6):301-309.

[7] Haque T, Packer JA, Zhao XL. Equivalent RHS approach for the design of EHS in axial compression or bending. Advances in Structural Engineering 2012;15(1):107-120.

[8] Insausti A, Gardner L. Analytical modelling of plastic collapse in compressed elliptical hollow sections. Journal of Constructional Steel Research 2011;67(4):678-689.

[9] Law KH, Gardner L. Lateral instability of elliptical hollow section beams. Engineering Structures 2012;37:152-166.

[10] Law KH, Gardner L. Buckling of elliptical hollow section members under combined compression and uniaxial bending. Journal of Constructional Steel Research 2013;86:1-16.

[11] Theofanous M, Chan TM, Gardner L. Structural response of stainless steel oval hollow section compression members. Engineering Structures 2009;31(4):922-934.

[12] Theofanous M, Chan TM, Gardner L. Flexural behaviour of stainless steel oval hollow sections. Thin-Walled Structures 2009;47(6):776-787.

[13] Chen MT, Young B. Material properties and structural behavior of cold-formed steel

elliptical hollow section stub columns. Thin-Walled Structures 2018; https://doi.org/10.1016/j.tws.2018.07.055 (In press).

[14] Chen MT, Young B. Tests of cold-formed steel elliptical hollow section beams. In: 7th International Conference on Coupled Instabilities in Metal Structures, Baltimore, Maryland, U.S.; Paper No. 48.

[15] AISI-S100 2016. North American Specification for the design of cold-formed steel structural members. *AISI S100-16.* Washington,D.C., USA: American Iron and Steel Institute.

[16] ANSI/AISC360 2016. Specification for Structural Steel Buildings. *ANSI/AISC 360-16.* Chicago, IL, USA: American Institute of Steel Construction.

[17] AS4100 1998. Steel structures. *AS 4100: 1998.* Homebush, New South Wales, Australia: Standards Australia.

[18] AS/NZS4600 2005. Cold-formed steel structure. *AS/NZS 4600:2005.* Sydney, Australia: Standards Australia/Standards New Zealand.

[19] EN1993-1-1 2005. Design of steel structures–Part 1.1: General rules and rules for buildings. *EN 1993-1-1:2005.* Brussels, Belgium: European Committee for Standardization.

[20] Chen MT, Young B. Cross-sectional behavior of cold-formed steel semi-oval hollow sections. Engineering Structures 2018;177:318-330.

[21] Huang Y, Young B. Experimental and numerical investigation of cold-formed lean duplex stainless steel flexural members. Thin-Walled Structures 2013;73:216-228.

[22] Huang Y, Young B. Structural performance of cold-formed lean duplex stainless steel columns. Thin-Walled Structures 2014;83:59-69.

[23] Ma JL, Chan TM, Young B. Experimental Investigation on Stub-Column Behavior of Cold-Formed High-Strength Steel Tubular Sections. Journal of Structural Engineering 2015;142(5):04015174.

[24] Zhao O, Rossi B, Gardner L, Young B. Behaviour of structural stainless steel cross-sections under combined loading–Part II: Numerical modelling and design approach. Engineering Structures 2015;89:247-259.

[25] Chen MT, Young B. Experimental and numerical investigation on pin-ended cold-formed steel semi-oval hollow section compression members. Journal of Constructional Steel Research 2018;151:174-184.

[26] Silvestre N. Buckling behaviour of elliptical cylindrical shells and tubes under compression. International Journal of Solids and Structures 2008;45(16):4427-4447.

[27] Silvestre N, Gardner L. Elastic local post-buckling of elliptical tubes. Journal of Constructional Steel Research 2011;67(3):281-292.

[28] Abela JM, Gardner L. Elastic buckling of elliptical tubes subjected to generalised linearly varying stress distributions. Thin-Walled Structures 2012;58:40-50.

[29] McCann F, Fang C, Gardner L, Silvestre N. Local buckling and ultimate strength of slender elliptical hollow sections in compression. Engineering Structures 2016;111:104-118.

[30] Schafer BW, Ádány S. Buckling analysis of cold-formed steel members using CUFSM: conventional and constrained finite strip methods. In: Eighteenth International Specialty Conference on Cold-Formed Steel Structures, Orlando, FL, USA; 2006. 39-54.

(a) Glass roof supporting members in International Finance Center in Hong Kong

(b) Glass facade supporting members in Heathrow Airport in London

Fig. 1. Structures employing EHS as structural supporting components

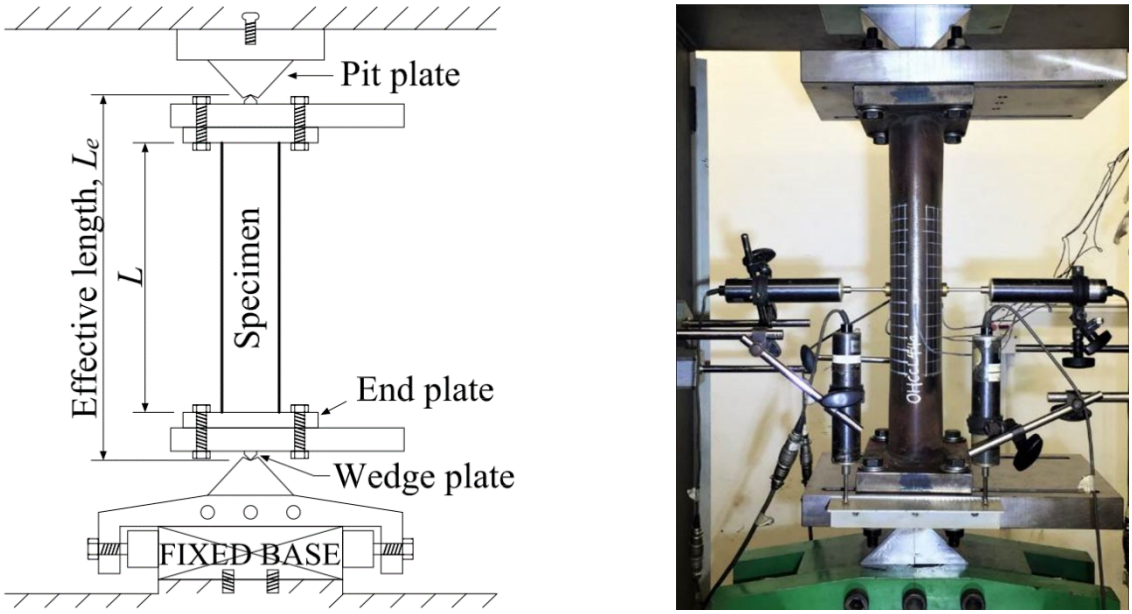

(a) Schematic view (b) Experimental arrangement

Fig. 2. Test setup and test rig for EHS pin-ended columns with actual specimen lengths of 200 and 440 mm

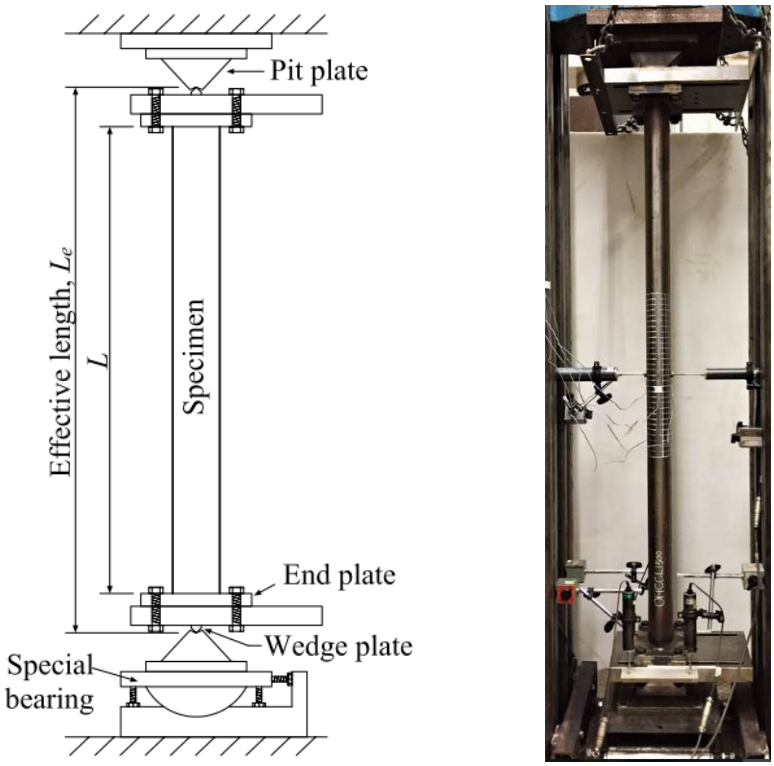

(a) Schematic view (b) Experimental arrangement

Fig. 3. Test setup and test rig for EHS pin-ended columns with actual specimen lengths of 850, 1200 and 1500 mm

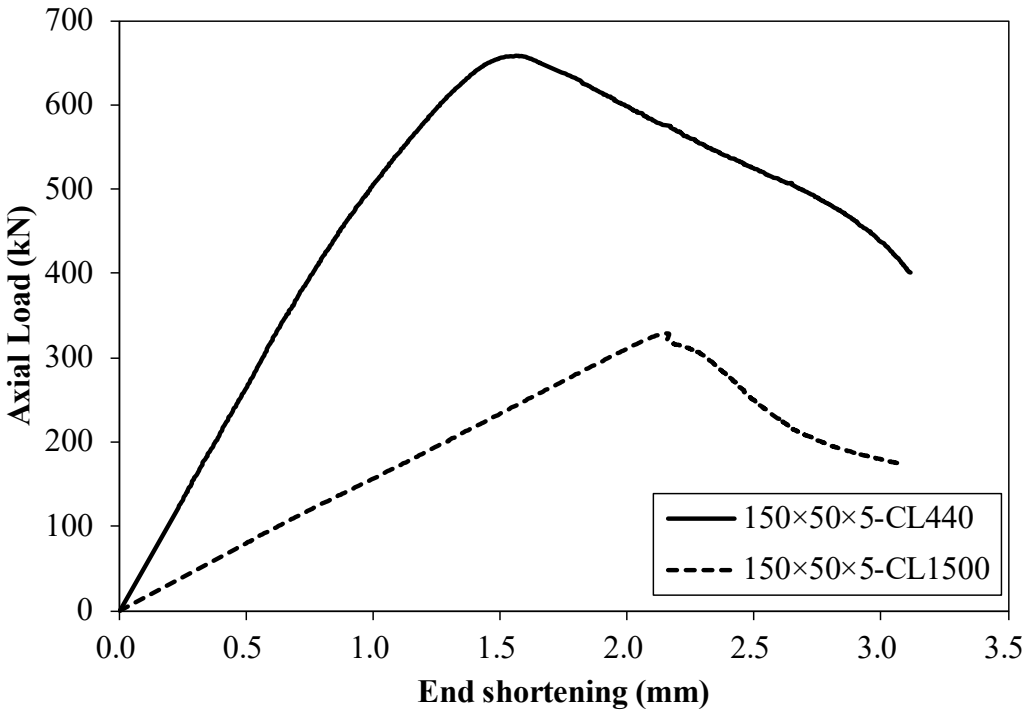

Fig. 4. Load-end shortening responses for typical EHS pin-ended column specimens 150×50×5-CL440 and 150×50×5-CL1500

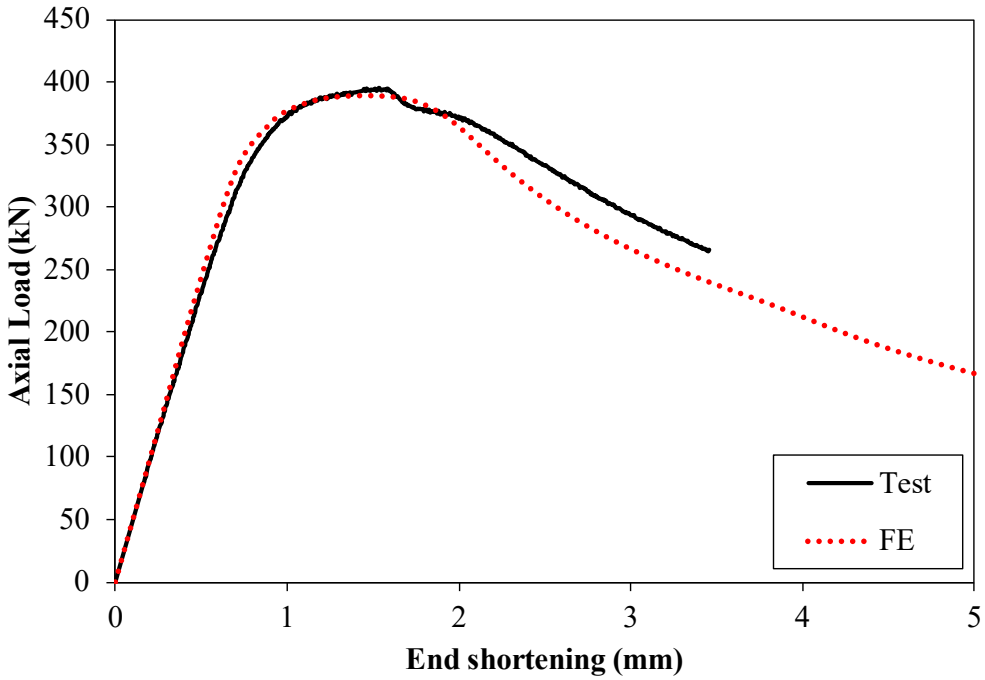

Fig. 5. Comparison between experimental and numerical load-end shortening responses for EHS column specimen 140×85×3-CL440 failed by local buckling

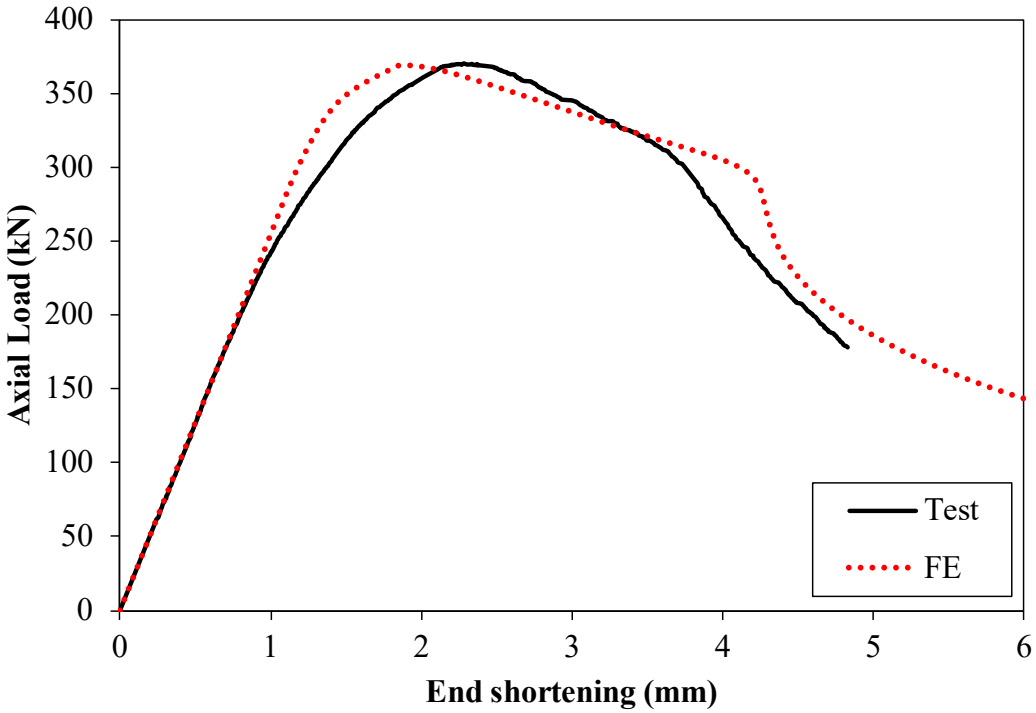

Fig. 6. Comparison between experimental and numerical load-end shortening responses for EHS column specimen 140×85×3-CL850 failed by interaction of local and flexural buckling

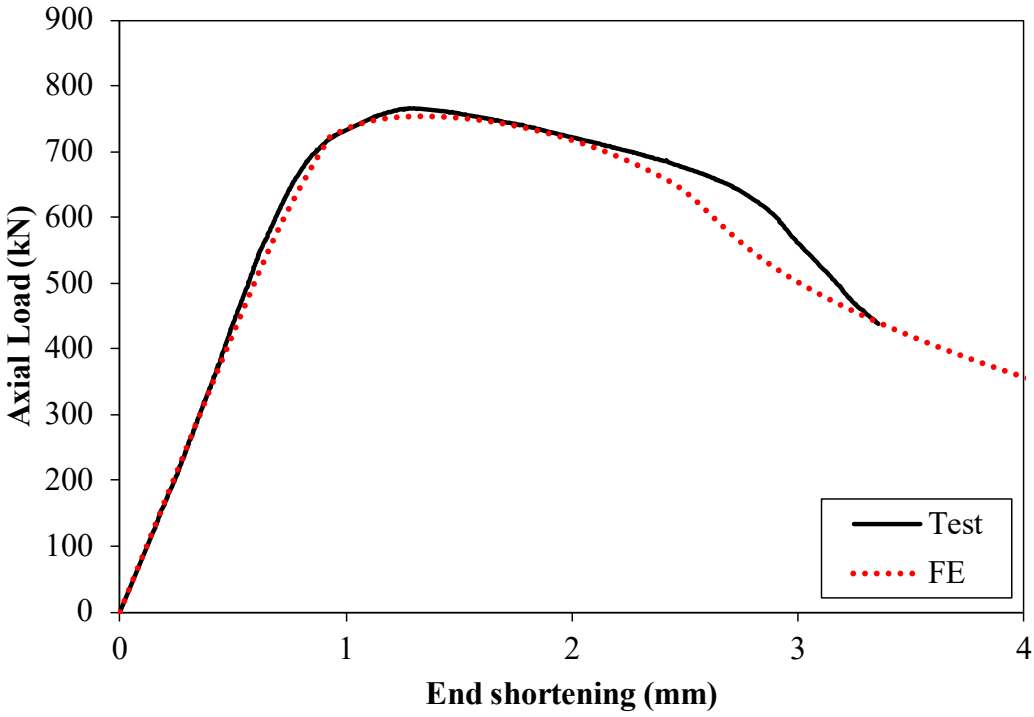

Fig. 7. Comparison between experimental and numerical load-end shortening responses for EHS column specimen 180×65×5-CL440 failed by material yielding

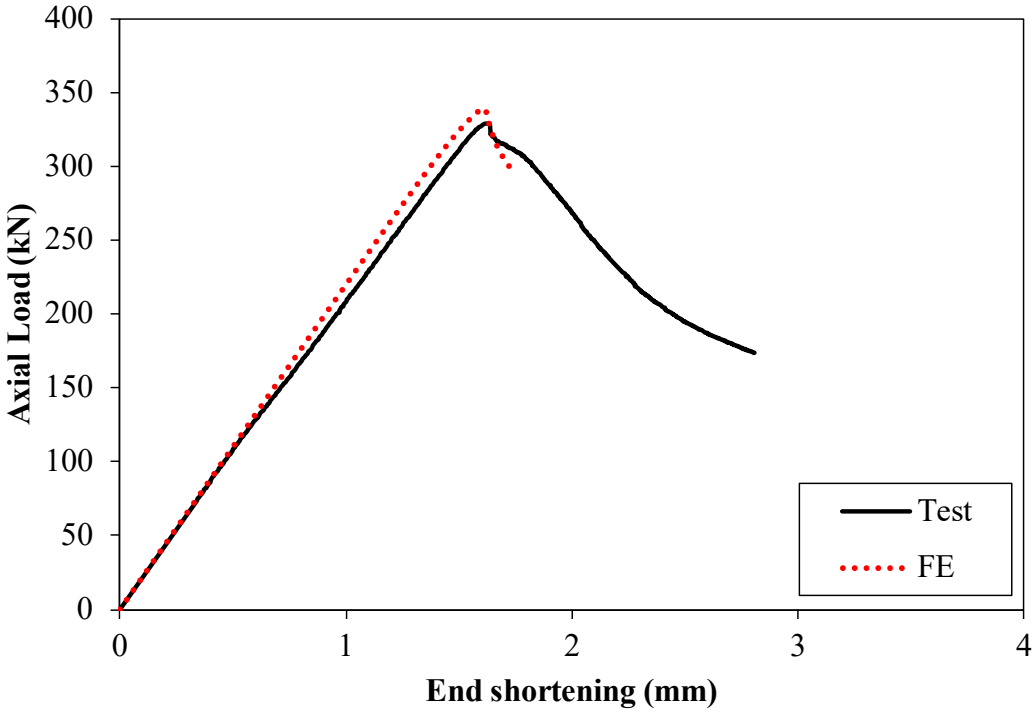

Fig. 8. Comparison between experimental and numerical load-end shortening responses for EHS column specimen 150×50×5-CL1500 failed by flexural buckling

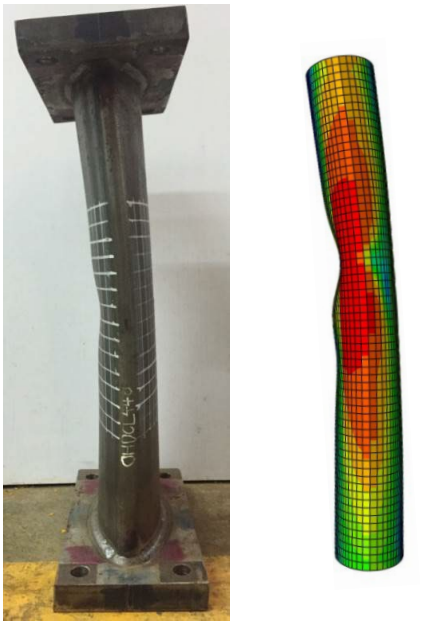

Fig. 9. Comparison between experimental and numerical failure modes for EHS column specimen 180×65×5-CL440 (Material yielding)

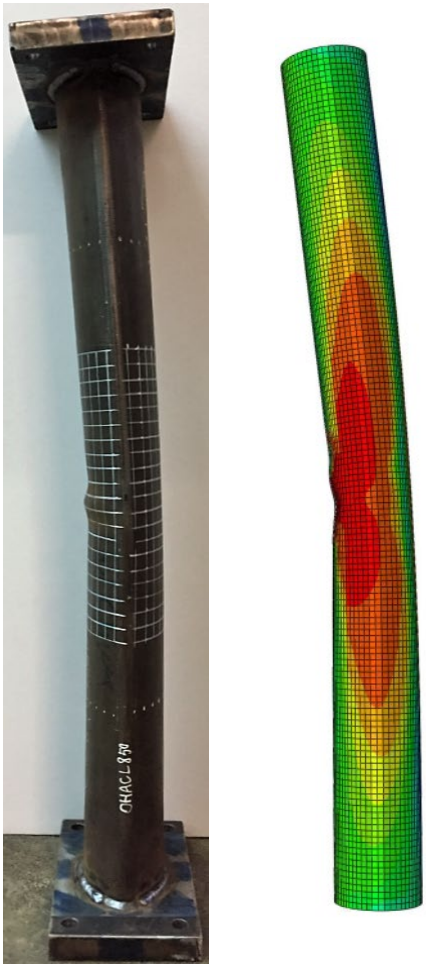

Fig. 10. Comparison between experimental and numerical failure modes for EHS column specimen 140×85×3-CL850 (Interaction of local and flexural buckling)

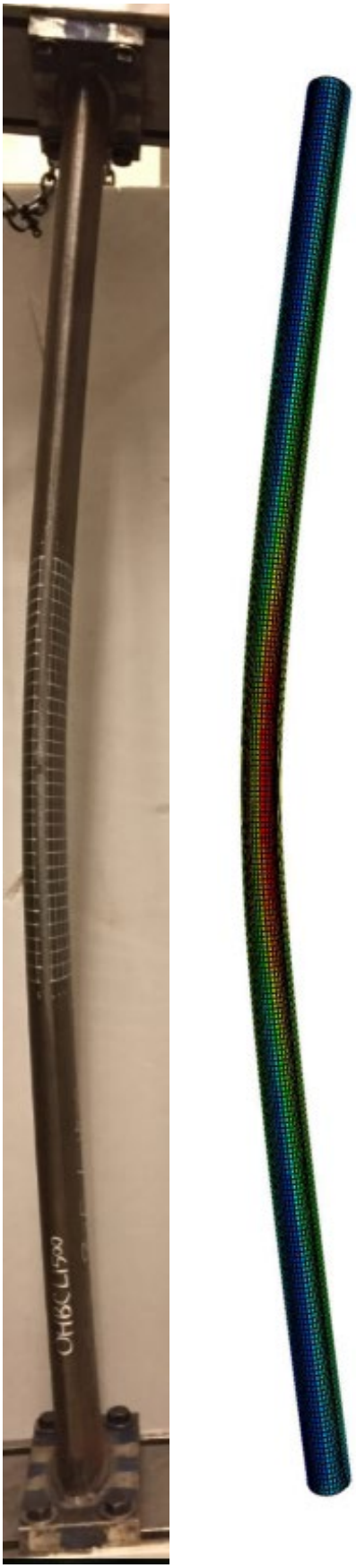

Fig. 11. Comparison between experimental and numerical failure modes for EHS column specimen 150×50×5-CL1500 (Flexural buckling)

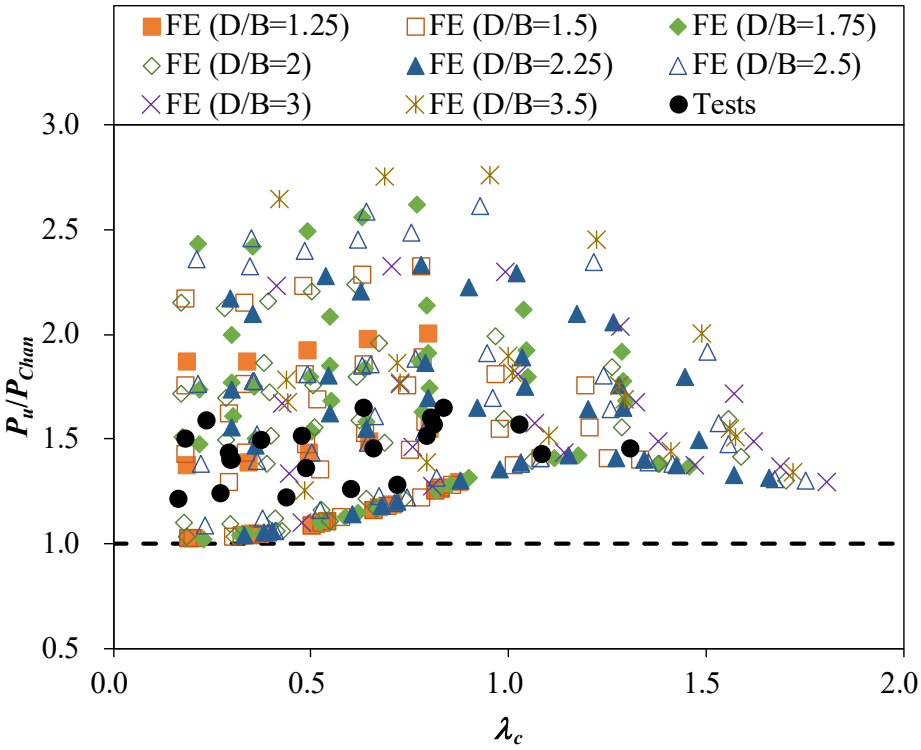

Fig. 12. Comparison of test and FE results with design strengths predicted by the equivalent diameter method

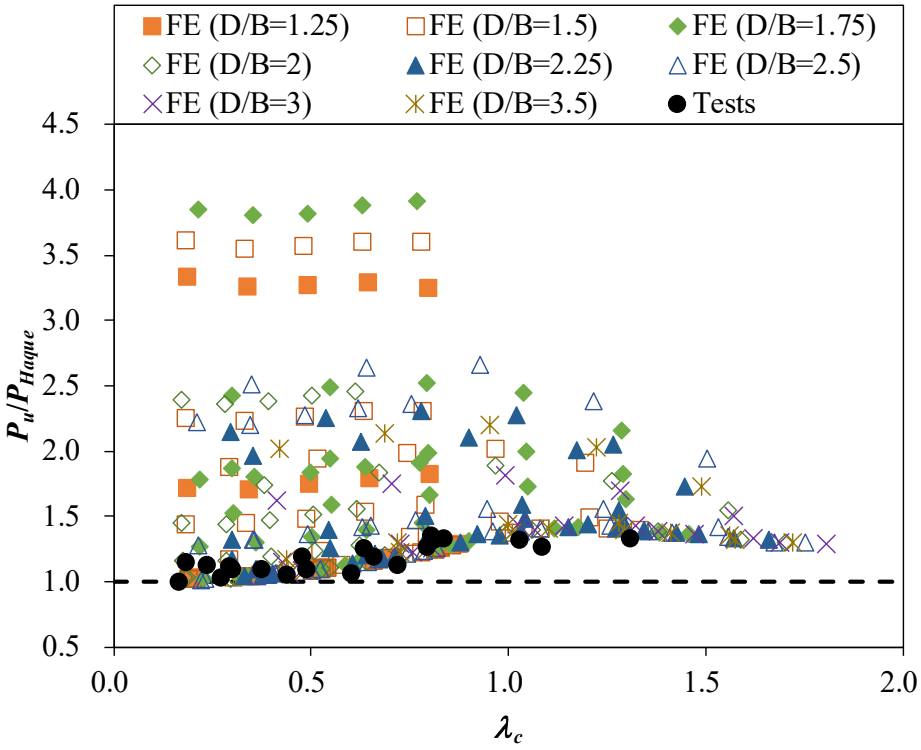

Fig. 13. Comparison of test and FE results with design strengths predicted by the equivalent RHS approach

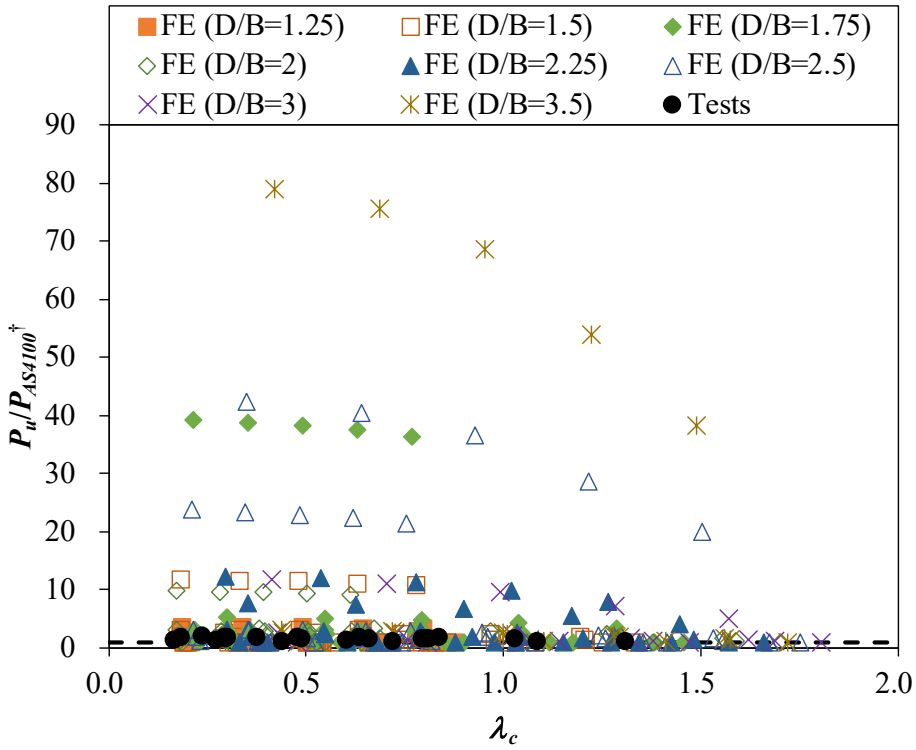

Fig. 14. Comparison of test and FE results with design strength predicted by the AS4100 [17] with equivalent diameter adopted

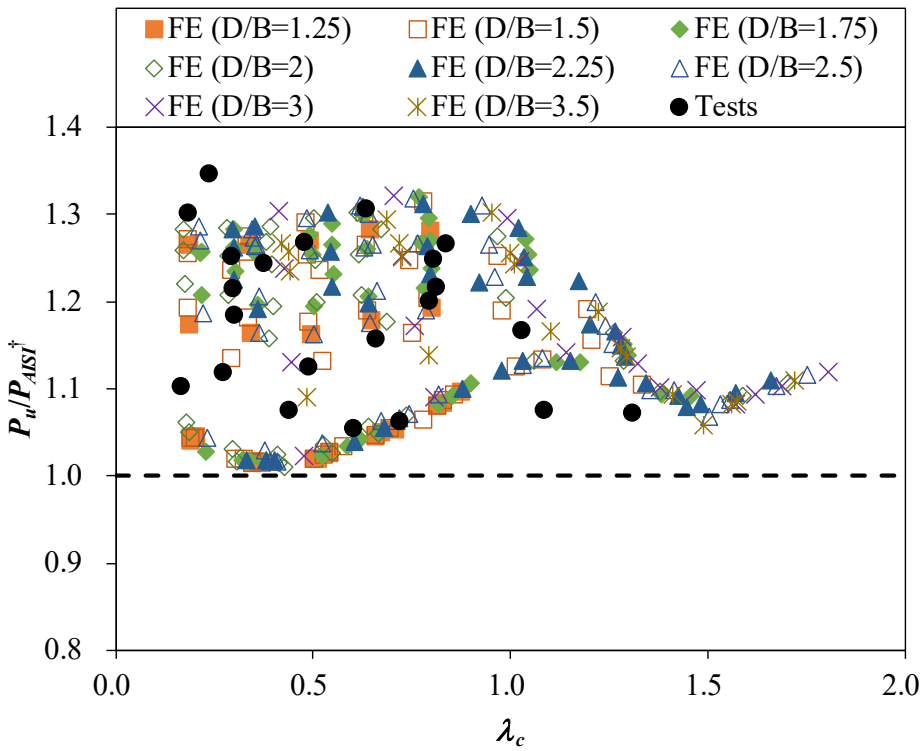

Fig. 15. Comparison of test and FE results with design strength predicted by the AISI-S100 [15] with equivalent diameter adopted

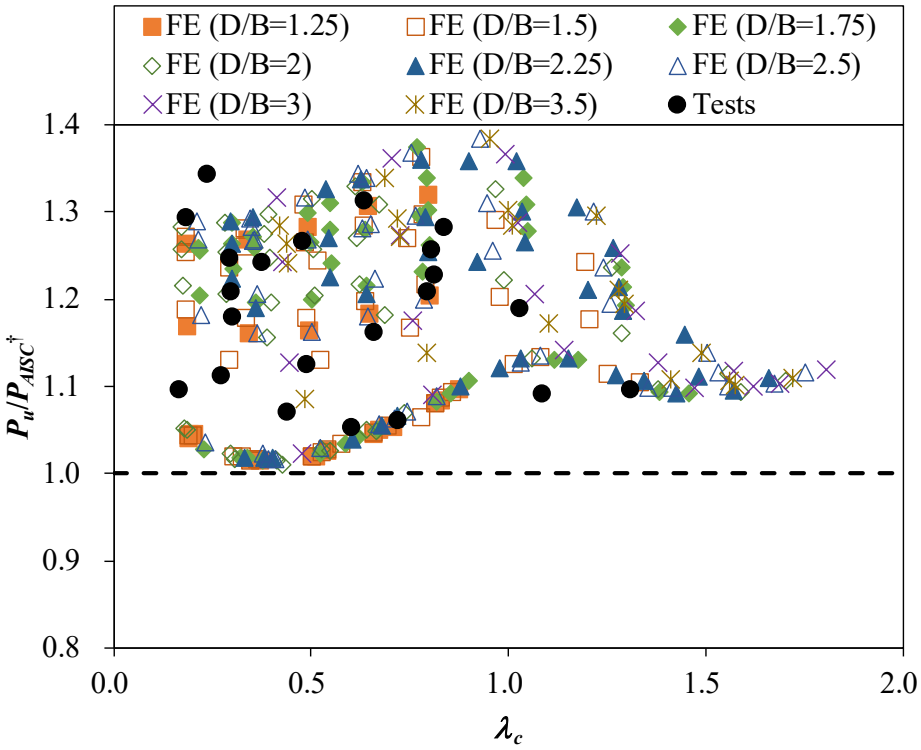

Fig. 16. Comparison of test and FE results with design strength predicted by the ANSI/AISC360 [16] with equivalent diameter adopted

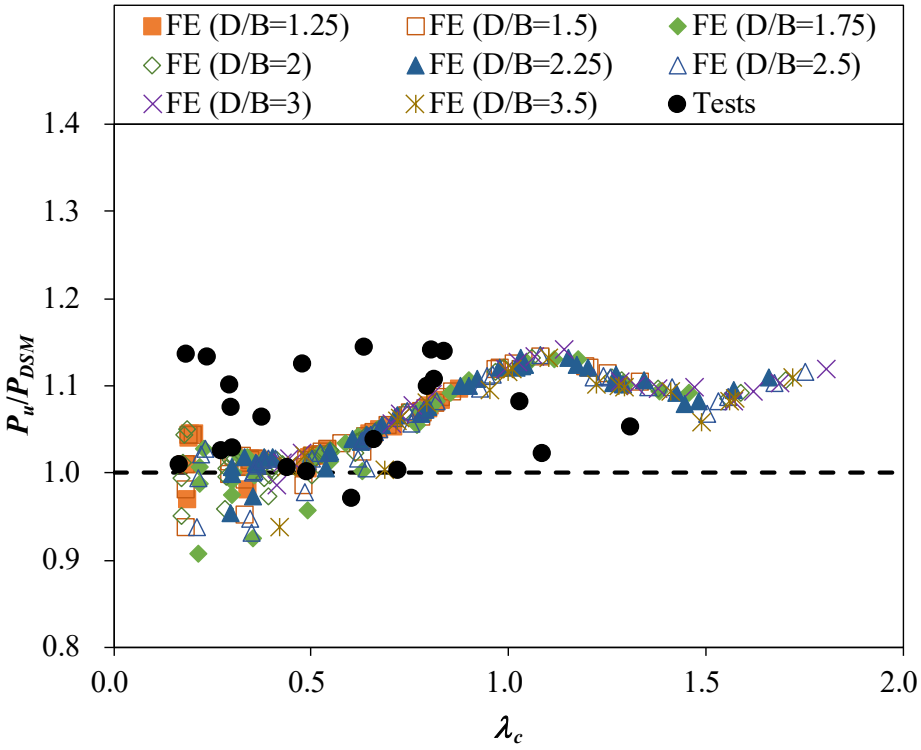

Fig. 17. Comparison of test and FE results with design strength predicted by the DSM

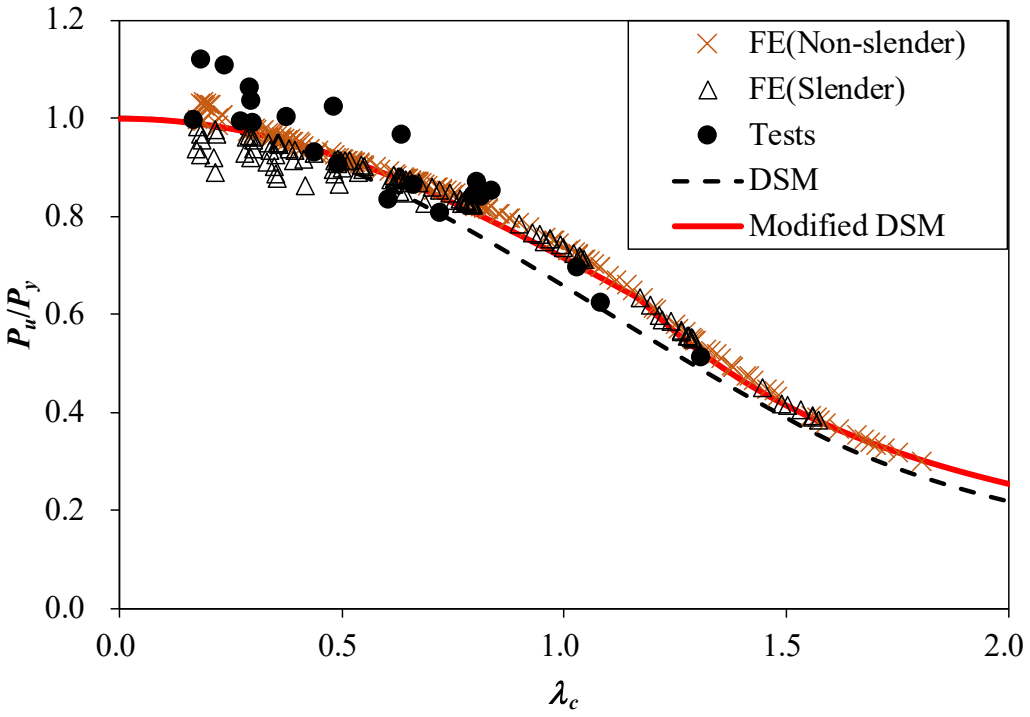

Fig. 18. Comparison of test and FE results with design curves of the existing and modified DSM

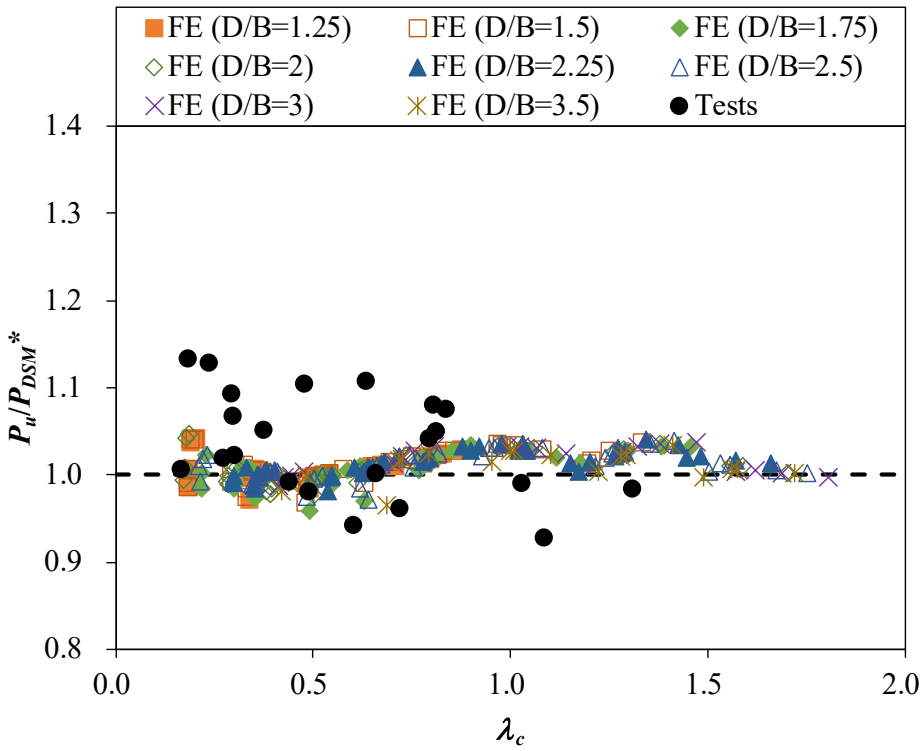

Fig. 19. Comparison of test and FE results with design strength predicted by the modified DSM

Section	Flattest Portion (TC1)						Curviest Portion (TC2)					
	E (GPa)	$\sigma_{0.2}$ (MPa)	σ_u (MPa)	ε_u (%)	ε_f (%)	n	E (GPa)	$\sigma_{0.2}$ (MPa)	σ_u (MPa)	ε_u (%)	ε_f (%)	n
140×85×3	208.0	388.4	432.9	4.5	13.9	21	212.7	401.0	457.8	3.7	12.7	17
150×50×5	204.7	409.6	521.2	9.9	20.3	38	213.4	529.0	653.8	4.8	12.2	6
150×70×3	210.4	341.4	392.5	5.4	15.7	23	210.3	339.8	396.8	4.1	13.6	19
180×65×5	200.4	417.7	499.4	9.1	18.7	N/A	206.4	532.8	635.1	3.8	12.2	6

Table 1. Measured material properties obtained from tensile coupon tests [13]

Specimen	D (mm)	B (mm)	t (mm)	L (mm)	ω_g (mm)	$\lvert\omega_g/L\rvert$
140×85×3-CL200	141.4	86.2	2.89	200	0	0
140×85×3-CL440	141.6	86.5	2.88	440	0	0
140×85×3-CL850	139.7	89.3	2.89	850	0	0
140×85×3-CL1200	141.2	86.6	2.74	1200	-0.38	1/3150
140×85×3-CL1500	140.5	88.5	2.91	1500	-0.44	1/3375
150×50×5-CL200	150.0	51.3	4.92	200	0	0
150×50×5-CL440	150.3	51.4	4.89	440	0.06	1/6929
150×50×5-CL850	150.2	51.7	4.93	850	-0.10	1/8924
150×50×5-CL1200	150.1	51.1	5.08	1200	-0.19	1/6299
150×50×5-CL1500	150.1	51.3	4.95	1500	-0.19	1/7874
150×70×3-CL200	149.4	71.2	2.82	200	0	0
150×70×3-CL440	148.3	72.6	2.83	440	-0.25	1/1732
150×70×3-CL440#	148.3	71.3	2.65	440	-0.32	1/1386
150×70×3-CL850	147.4	73.1	2.70	850	-0.32	1/2677
150×70×3-CL1200	148.3	72.5	2.67	1200	-0.29	1/4108
150×70×3-CL1500	148.1	71.9	2.67	1500	0.22	1/6749
150×70×3-CL1500#	147.7	72.6	2.70	1500	-0.34	1/4374
180×65×5-CL200	177.2	63.8	4.72	200	0	0
180×65×5-CL440	176.4	66.0	4.72	440	0.25	1/1732
180×65×5-CL850	176.6	65.0	4.82	850	0.06	1/13386
180×65×5-CL1200	176.5	66.0	4.79	1200	-0.51	1/2362
180×65×5-CL1500	176.5	65.5	4.82	1500	0.38	1/3937

Table 2. Measured dimensions and initial global geometric imperfections of EHS pin-ended columns

Specimen	$e+\omega_g$ (mm)	L_e (mm)	P_{Exp} (kN)	Failure mode	P_y (kN)	$\frac{P_{Exp}}{P_y}$
140×85×3-CL200	0.11	374	396.5	L	396.7	1.00
140×85×3-CL440	0.38	614	394.6	L	396.1	1.00
140×85×3-CL850	0.43	1024	370.8	L+F	398.3	0.93
140×85×3-CL1200	0.09	1374	314.9	L+F	377.8	0.83
140×85×3-CL1500	0.24	1674	324.6	L+F	401.8	0.81
150×50×5-CL200	0.08	374	687.7	Y	647.5	1.06
150×50×5-CL440	0.03	614	659.2	Y	644.8	1.02
150×50×5-CL850	0.24	1024	548.5	F	650.5	0.84
150×50×5-CL1200	0.01	1374	417.7	F	667.1	0.63
150×50×5-CL1500	0.12	1674	335.1	F	651.4	0.51
150×70×3-CL200	0.12	374	376.8	Y	333.9	1.13
150×70×3-CL440	1.04	614	349.5	Y	335.7	1.04
150×70×3-CL440#	0.41	614	312.1	Y	313.2	1.00
150×70×3-CL850	0.31	1024	290.7	F	319.5	0.91
150×70×3-CL1200	0.18	1374	275.4	F	317.1	0.87
150×70×3-CL1500	0.33	1674	267.0	F	316.0	0.84
150×70×3-CL1500#	0.14	1674	279.3	F	319.6	0.87
180×65×5-CL200	0.47	374	843.3	Y	761.3	1.11
180×65×5-CL440	0.26	614	766.1	Y	763.4	1.00
180×65×5-CL850	0.26	1024	751.9	F	776.6	0.97
180×65×5-CL1200	0.31	1374	659.1	F	774.4	0.85
180×65×5-CL1500	0.06	1674	541.1	F	778.2	0.70

Table 3. Test results of EHS pin-ended column specimens

Specimen	P_{Exp}/P_{FE} Material division				P_{Exp}/P_{FE} Local imperfection+Global imperfection			
	$D_m/3$	$D_m/4$	$D_m/6$	$D_m/10$	$t/3+L/3500$	$t/10+L/3500$	$t/50+L/3500$	$t/100+L/3500$
140×85×3-CL200	0.94	0.96	0.97	0.98	1.09	1.00	**0.97**	0.96
140×85×3-CL440	1.00	1.01	1.02	1.02	1.13	1.04	**1.01**	1.02
140×85×3-CL850	1.00	1.00	1.01	1.01	1.06	1.00	**1.01**	1.01
140×85×3-CL1200	0.95	0.95	0.95	0.94	1.09	1.00	**0.99**	0.99
140×85×3-CL1500	0.97	0.97	0.97	0.97	1.12	1.02	**1.01**	1.01
150×50×5-CL200	0.87	0.92	0.97	1.01	1.07	0.99	**0.98**	0.97
150×50×5-CL440	1.02	1.06	1.11	1.14	1.16	1.11	**1.11**	1.11
150×50×5-CL850	0.98	1.00	1.00	0.99	1.16	1.09	**1.09**	1.09
150×50×5-CL1200	0.87	0.85	0.83	0.82	0.97	0.96	**0.96**	0.96
150×50×5-CL1500	0.91	0.91	0.90	0.90	1.00	0.99	**0.99**	0.99
150×70×3-CL200	1.13	1.13	1.14	1.14	1.26	1.17	**1.14**	1.14
150×70×3-CL440	1.14	1.14	1.14	1.14	1.27	1.17	**1.15**	1.14
150×70×3-CL440#	1.07	1.07	1.07	1.07	1.20	1.10	**1.08**	1.08
150×70×3-CL850	1.04	1.04	1.04	1.04	1.06	0.97	**0.95**	0.95
150×70×3-CL1200	1.04	1.04	1.04	1.03	1.20	1.10	**1.09**	1.09
150×70×3-CL1500	1.09	1.08	1.08	1.07	1.17	1.07	**1.05**	1.05
150×70×3-CL1500#	1.08	1.08	1.07	1.06	1.30	1.17	**1.14**	1.14
180×65×5-CL200	0.92	0.97	1.02	1.06	1.15	1.05	**1.03**	1.02
180×65×5-CL440	0.93	0.97	1.02	1.04	1.13	1.04	**1.02**	1.02
180×65×5-CL850	1.00	1.02	1.02	1.01	1.22	1.11	**1.09**	1.08
180×65×5-CL1200	0.95	0.93	0.92	0.91	1.19	1.04	**1.01**	1.01
180×65×5-CL1500	0.93	0.91	0.88	0.87	0.98	0.86	**0.83**	0.83
Mean	0.99	1.00	1.01	1.01	1.14	1.05	**1.03**	1.03
COV	0.078	0.076	0.079	0.084	0.080	0.073	**0.073**	0.073

Table 4. Summary of sensitivity study of EHS pin-ended columns

Specimen	D/B	L_e (mm)	P_{FE} (kN)	Specimen	D/B	L_e (mm)	P_{FE} (kN)
250×200×20-CL800	1.25	973.6	5161.3	150×75×8-CL600	2.00	773.6	994.1
250×200×20-CL1600	1.25	1773.6	4811.9	150×75×8-CL1200	2.00	1373.6	897.8
250×200×20-CL2400	1.25	2573.6	4561.5	150×75×8-CL1800	2.00	1973.6	745.9
250×200×20-CL3200	1.25	3373.6	4290.2	150×75×8-CL2400	2.00	2573.6	519.9
250×200×20-CL4000	1.25	4173.6	3996.7	150×75×8-CL3000	2.00	3173.6	352.3
250×200×10-CL800	1.25	973.6	2710.1	150×75×3-CL600	2.00	773.6	393.0
250×200×10-CL1600	1.25	1773.6	2540.3	150×75×3-CL1200	2.00	1373.6	357.3
250×200×10-CL2400	1.25	2573.6	2407.0	150×75×3-CL1800	2.00	1973.6	307.5
250×200×10-CL3200	1.25	3373.6	2289.6	150×75×3-CL2400	2.00	2573.6	227.8
250×200×10-CL4000	1.25	4173.6	2138.7	150×75×3-CL3000	2.00	3173.6	156.5
250×200×6-CL800	1.25	973.6	1648.6	150×75×3-CL600	2.00	773.6	195.5
250×200×6-CL1600	1.25	1773.6	1555.8	150×75×3-CL1200	2.00	1373.6	181.6
250×200×6-CL2400	1.25	2573.6	1475.9	150×75×3-CL1800	2.00	1973.6	157.5
250×200×6-CL3200	1.25	3373.6	1403.1	150×75×3-CL2400	2.00	2573.6	118.9
250×200×6-CL4000	1.25	4173.6	1317.2	150×75×3-CL3000	2.00	3173.6	82.0
250×200×3-CL800	1.25	973.6	811.2	270×120×16-CL800	2.25	973.6	3545.3
250×200×3-CL1600	1.25	1773.6	782.6	270×120×16-CL1600	2.25	1773.6	3251.2
250×200×3-CL2400	1.25	2573.6	748.7	270×120×16-CL2400	2.25	2573.6	2904.8
250×200×3-CL3200	1.25	3373.6	715.1	270×120×16-CL3200	2.25	3373.6	2365.9
250×200×3-CL4000	1.25	4173.6	670.9	270×120×16-CL4000	2.25	4173.6	1699.7
250×200×1.5-CL800	1.25	973.6	392.1	270×120×4.5-CL800	2.25	973.6	1053.7
250×200×1.5-CL1600	1.25	1773.6	383.8	270×120×4.5-CL1600	2.25	1773.6	981.7
250×200×1.5-CL2400	1.25	2573.6	372.7	270×120×4.5-CL2400	2.25	2573.6	896.7
250×200×1.5-CL3200	1.25	3373.6	359.1	270×120×4.5-CL3200	2.25	3373.6	774.8
250×200×1.5-CL4000	1.25	4173.6	338.0	270×120×4.5-CL4000	2.25	4173.6	596.4
300×200×20-CL800	1.50	973.6	5830.9	270×120×3.5-CL800	2.25	973.6	817.1
300×200×20-CL1600	1.50	1773.6	5459.7	270×120×3.5-CL1600	2.25	1773.6	767.6
300×200×20-CL2400	1.50	2573.6	5175.9	270×120×3.5-CL2400	2.25	2573.6	702.4
300×200×20-CL3200	1.50	3373.6	4903.7	270×120×3.5-CL3200	2.25	3373.6	609.5
300×200×20-CL4000	1.50	4173.6	4564.3	270×120×3.5-CL4000	2.25	4173.6	472.1
300×200×10-CL800	1.50	973.6	3045.2	270×120×2-CL800	2.25	973.6	450.1
300×200×10-CL1600	1.50	1773.6	2857.8	270×120×2-CL1600	2.25	1773.6	435.2
300×200×10-CL2400	1.50	2573.6	2715.2	270×120×2-CL2400	2.25	2573.6	404.7
300×200×10-CL3200	1.50	3373.6	2586.2	270×120×2-CL3200	2.25	3373.6	353.7
300×200×10-CL4000	1.50	4173.6	2424.1	270×120×2-CL4000	2.25	4173.6	276.3
300×200×4-CL800	1.50	973.6	1207.6	180×80×12-CL600	2.25	773.6	1718.7
300×200×4-CL1600	1.50	1773.6	1164.7	180×80×12-CL1200	2.25	1373.6	1552.4
300×200×4-CL2400	1.50	2573.6	1114.3	180×80×12-CL1800	2.25	1973.6	1309.7
300×200×4-CL3200	1.50	3373.6	1065.7	180×80×12-CL2400	2.25	2573.6	937.6

300×200×4-CL4000	1.50	4173.6	1003.7	180×80×12-CL3000	2.25	3173.6	638.9
300×200×4-CL800	1.50	973.6	737.9	180×80×8-CL600	2.25	773.6	1188.3
300×200×4-CL1600	1.50	1773.6	722.9	180×80×8-CL1200	2.25	1373.6	1079.3
300×200×4-CL2400	1.50	2573.6	697.0	180×80×8-CL1800	2.25	1973.6	933.9
300×200×4-CL3200	1.50	3373.6	670.3	180×80×8-CL2400	2.25	2573.6	700.8
300×200×4-CL4000	1.50	4173.6	631.2	180×80×8-CL3000	2.25	3173.6	483.8
300×200×1.5-CL800	1.50	973.6	425.1	180×80×3.5-CL600	2.25	773.6	537.7
300×200×1.5-CL1600	1.50	1773.6	418.2	180×80×3.5-CL1200	2.25	1373.6	493.6
300×200×1.5-CL2400	1.50	2573.6	411.5	180×80×3.5-CL1800	2.25	1973.6	436.1
300×200×1.5-CL3200	1.50	3373.6	398.4	180×80×3.5-CL2400	2.25	2573.6	344.2
300×200×1.5-CL4000	1.50	4173.6	381.4	180×80×3.5-CL3000	2.25	3173.6	242.5
150×100×12-CL600	1.50	773.6	1635.2	180×80×3.5-CL600	2.25	773.6	225.7
150×100×12-CL1200	1.50	1373.6	1508.3	180×80×3.5-CL1200	2.25	1373.6	214.7
150×100×12-CL1800	1.50	1973.6	1367.0	180×80×3.5-CL1800	2.25	1973.6	191.5
150×100×12-CL2400	1.50	2573.6	1165.4	180×80×3.5-CL2400	2.25	2573.6	154.4
150×100×12-CL3000	1.50	3173.6	880.1	180×80×3.5-CL3000	2.25	3173.6	109.8
150×100×6-CL600	1.50	773.6	863.7	500×200×20-CL1000	2.50	1173.6	8518.4
150×100×6-CL1200	1.50	1373.6	800.4	500×200×20-CL1750	2.50	1923.6	8102.4
150×100×6-CL1800	1.50	1973.6	728.3	500×200×20-CL2500	2.50	2673.6	7721.9
150×100×6-CL2400	1.50	2573.6	644.8	500×200×20-CL3250	2.50	3423.6	7361.9
150×100×6-CL3000	1.50	3173.6	510.6	500×200×20-CL4000	2.50	4173.6	6925.2
150×100×2.5-CL600	1.50	773.6	369.0	500×200×12-CL1000	2.50	1173.6	5202.9
150×100×2.5-CL1200	1.50	1373.6	344.2	500×200×12-CL1750	2.50	1923.6	4961.0
150×100×2.5-CL1800	1.50	1973.6	319.0	500×200×12-CL2500	2.50	2673.6	4752.8
150×100×2.5-CL2400	1.50	2573.6	283.3	500×200×12-CL3250	2.50	3423.6	4551.0
150×100×2.5-CL3000	1.50	3173.6	230.1	500×200×12-CL4000	2.50	4173.6	4301.2
150×100×2.5-CL600	1.50	773.6	220.2	500×200×7-CL1000	2.50	1173.6	2995.1
150×100×2.5-CL1200	1.50	1373.6	208.5	500×200×7-CL1750	2.50	1923.6	2915.7
150×100×2.5-CL1800	1.50	1973.6	193.2	500×200×7-CL2500	2.50	2673.6	2811.3
150×100×2.5-CL2400	1.50	2573.6	172.5	500×200×7-CL3250	2.50	3423.6	2701.2
150×100×2.5-CL3000	1.50	3173.6	141.0	500×200×7-CL4000	2.50	4173.6	2564.5
350×200×14-CL1000	1.75	1173.6	4572.6	500×200×3.5-CL1000	2.50	1173.6	1426.3
350×200×14-CL1750	1.75	1923.6	4350.8	500×200×3.5-CL1750	2.50	1923.6	1397.2
350×200×14-CL2500	1.75	2673.6	4150.5	500×200×3.5-CL2500	2.50	2673.6	1375.6
350×200×14-CL3250	1.75	3423.6	3958.5	500×200×3.5-CL3250	2.50	3423.6	1342.0
350×200×14-CL4000	1.75	4173.6	3722.2	500×200×3.5-CL4000	2.50	4173.6	1291.6
350×200×5-CL1000	1.75	1173.6	1655.9	250×100×16-CL800	2.50	973.6	3109.8
350×200×5-CL1750	1.75	1923.6	1598.7	250×100×16-CL1600	2.50	1773.6	2786.2
350×200×5-CL2500	1.75	2673.6	1536.5	250×100×16-CL2400	2.50	2573.6	2283.9
350×200×5-CL3250	1.75	3423.6	1473.2	250×100×16-CL3200	2.50	3373.6	1555.9
350×200×5-CL4000	1.75	4173.6	1393.0	250×100×16-CL4000	2.50	4173.6	1045.4
350×200×5-CL1000	1.75	1173.6	1143.8	250×100×12-CL800	2.50	973.6	2397.9

350×200×5-CL1750	1.75	1923.6	1116.4	250×100×12-CL1600	2.50	1773.6	2161.4
350×200×5-CL2500	1.75	2673.6	1079.7	250×100×12-CL2400	2.50	2573.6	1813.8
350×200×5-CL3250	1.75	3423.6	1037.6	250×100×12-CL3200	2.50	3373.6	1282.4
350×200×5-CL4000	1.75	4173.6	984.7	250×100×12-CL4000	2.50	4173.6	867.3
350×200×1.5-CL1000	1.75	1173.6	453.6	250×100×5-CL800	2.50	973.6	1039.6
350×200×1.5-CL1750	1.75	1923.6	447.9	250×100×5-CL1600	2.50	1773.6	948.8
350×200×1.5-CL2500	1.75	2673.6	441.4	250×100×5-CL2400	2.50	2573.6	823.5
350×200×1.5-CL3250	1.75	3423.6	433.0	250×100×5-CL3200	2.50	3373.6	622.1
350×200×1.5-CL4000	1.75	4173.6	420.6	250×100×5-CL4000	2.50	4173.6	428.1
210×120×16-CL800	1.75	973.6	2887.9	250×100×3.5-CL800	2.50	973.6	729.3
210×120×16-CL1600	1.75	1773.6	2640.8	250×100×3.5-CL1600	2.50	1773.6	671.4
210×120×16-CL2400	1.75	2573.6	2345.7	250×100×3.5-CL2400	2.50	2573.6	586.6
210×120×16-CL3200	1.75	3373.6	1881.5	250×100×3.5-CL3200	2.50	3373.6	448.7
210×120×16-CL4000	1.75	4173.6	1335.2	250×100×3.5-CL4000	2.50	4173.6	310.1
210×120×10-CL800	1.75	973.6	1881.8	250×100×1.5-CL800	2.50	973.6	294.4
210×120×10-CL1600	1.75	1773.6	1729.8	250×100×1.5-CL1600	2.50	1773.6	281.9
210×120×10-CL2400	1.75	2573.6	1556.3	250×100×1.5-CL2400	2.50	2573.6	254.5
210×120×10-CL3200	1.75	3373.6	1296.1	250×100×1.5-CL3200	2.50	3373.6	198.9
210×120×10-CL4000	1.75	4173.6	949.2	250×100×1.5-CL4000	2.50	4173.6	137.7
210×120×2.5-CL800	1.75	973.6	486.8	150×50×8-CL400	3.00	573.6	897.9
210×120×2.5-CL1600	1.75	1773.6	455.7	150×50×8-CL800	3.00	973.6	800.5
210×120×2.5-CL2400	1.75	2573.6	414.0	150×50×8-CL1200	3.00	1373.6	639.4
210×120×2.5-CL3200	1.75	3373.6	359.2	150×50×8-CL1600	3.00	1773.6	427.7
210×120×2.5-CL4000	1.75	4173.6	275.4	150×50×8-CL2000	3.00	2173.6	290.8
210×120×2-CL800	1.75	973.6	386.8	150×50×5-CL400	3.00	573.6	580.1
210×120×2-CL1600	1.75	1773.6	365.6	150×50×5-CL800	3.00	973.6	526.1
210×120×2-CL2400	1.75	2573.6	334.0	150×50×5-CL1200	3.00	1373.6	436.5
210×120×2-CL3200	1.75	3373.6	289.1	150×50×5-CL1600	3.00	1773.6	307.0
210×120×2-CL4000	1.75	4173.6	222.3	150×50×5-CL2000	3.00	2173.6	210.3
210×120×1.5-CL800	1.75	973.6	286.1	150×50×3-CL400	3.00	573.6	355.3
210×120×1.5-CL1600	1.75	1773.6	272.7	150×50×3-CL800	3.00	973.6	324.6
210×120×1.5-CL2400	1.75	2573.6	251.2	150×50×3-CL1200	3.00	1373.6	275.4
210×120×1.5-CL3200	1.75	3373.6	218.1	150×50×3-CL1600	3.00	1773.6	200.8
210×120×1.5-CL4000	1.75	4173.6	168.1	150×50×3-CL2000	3.00	2173.6	138.5
500×250×25-CL1000	2.00	1173.6	11397.6	150×50×3-CL400	3.00	573.6	176.2
500×250×25-CL1750	2.00	1923.6	10763.6	150×50×3-CL800	3.00	973.6	164.9
500×250×25-CL2500	2.00	2673.6	10312.6	150×50×3-CL1200	3.00	1373.6	142.4
500×250×25-CL3250	2.00	3423.6	9972.7	150×50×3-CL1600	3.00	1773.6	106.6
500×250×25-CL4000	2.00	4173.6	9592.7	150×50×3-CL2000	3.00	2173.6	73.8
500×250×16-CL1000	2.00	1173.6	7442.7	350×100×16-CL1000	3.50	1173.6	4116.0
500×250×16-CL1750	2.00	1923.6	7070.0	350×100×16-CL1750	3.50	1923.6	3697.7
500×250×16-CL2500	2.00	2673.6	6791.7	350×100×16-CL2500	3.50	2673.6	3029.9

500×250×16-CL3250	2.00	3423.6	6569.0	350×100×16-CL3250	3.50	3423.6	2114.2
500×250×16-CL4000	2.00	4173.6	6339.5	350×100×16-CL4000	3.50	4173.6	1463.2
500×250×8-CL1000	2.00	1173.6	3680.7	350×100×8-CL1000	3.50	1173.6	2135.2
500×250×8-CL1750	2.00	1923.6	3583.5	350×100×8-CL1750	3.50	1923.6	1959.2
500×250×8-CL2500	2.00	2673.6	3460.9	350×100×8-CL2500	3.50	2673.6	1677.9
500×250×8-CL3250	2.00	3423.6	3363.7	350×100×8-CL3250	3.50	3423.6	1254.4
500×250×8-CL4000	2.00	4173.6	3254.2	350×100×8-CL4000	3.50	4173.6	881.3
500×250×6-CL1000	2.00	1173.6	2728.4	350×100×7-CL1000	3.50	1173.6	1876.4
500×250×6-CL1750	2.00	1923.6	2675.6	350×100×7-CL1750	3.50	1923.6	1724.6
500×250×6-CL2500	2.00	2673.6	2598.4	350×100×7-CL2500	3.50	2673.6	1484.7
500×250×6-CL3250	2.00	3423.6	2534.3	350×100×7-CL3250	3.50	3423.6	1119.5
500×250×6-CL4000	2.00	4173.6	2455.9	350×100×7-CL4000	3.50	4173.6	788.1
500×250×3.5-CL1000	2.00	1173.6	1531.3	350×100×2.5-CL1000	3.50	1173.6	633.1
500×250×3.5-CL1750	2.00	1923.6	1513.5	350×100×2.5-CL1750	3.50	1923.6	604.8
500×250×3.5-CL2500	2.00	2673.6	1489.5	350×100×2.5-CL2500	3.50	2673.6	548.7
500×250×3.5-CL3250	2.00	3423.6	1465.5	350×100×2.5-CL3250	3.50	3423.6	432.2
500×250×3.5-CL4000	2.00	4173.6	1427.2	350×100×2.5-CL4000	3.50	4173.6	306.4

Table 5. Parametric study on cold-formed steel EHS pin-ended columns buckled about the minor axis

Number of Test:22	FE: 280	$\frac{P_u}{P_{Chan}}$	$\frac{P_u}{P_{Haque}}$	$\frac{P_u}{P_{AS4100}^{\dagger}}$	$\frac{P_u}{P_{AISI}^{\dagger}}$	$\frac{P_u}{P_{AISC}^{\dagger}}$	$\frac{P_u}{P_{DSM}}$	$\frac{P_u}{P_{DSM}}$ *
ALL: 302	Mean	1.59	1.56	4.97	1.17	1.18	1.05	**1.01**
	COV	0.251	0.387	2.106	0.081	0.089	0.048	**0.023**
	ϕ	1.00	1.00	0.90	0.85	0.90	0.85	**0.85**
	β	2.71	2.02	1.02	3.30	3.09	3.00	**2.88**

†: Nominal design strengths predicted by adopting the equivalent diameter proposed by Chan *et al.* [4]
*: Modified design method

Table 6. Comparison of EHS pin-ended column test and FE results with predicted strengths